An Acad Bras Cienc (2024) 96(4): e20240120 DOI 10.1590/0001-3765202420240120
Anais da Academia Brasileira de Ciências | *Annals of the Brazilian Academy of Sciences*
Printed ISSN 0001-3765 I Online ISSN 1678-2690
www.scielo.br/aabc | www.fb.com/aabcjournal

HEALTH SCIENCES

The changes of peripheral blood hub genes in 24-week-old APP/PS1/Tau triple transgenic mouse model based on weighted gene co-expression network analysis

HEXU LIU, CHANGYIN YU & CHAO QIN

Abstract: Peripheral regulation emerges as a promising intervention in the early stages of Alzheimer's disease (AD). The hub genes in the peripheral blood of MCI patients from GEO database (GSE63060, GSE63061) were screened using weighted gene co-expression analysis (WGCNA). Meanwhile, behavioral tests, HE staining and Nissl staining were used to detect the memory impairment and histopathological changes in 24-week-old male 3×Tg-AD mice. Thioflavin-S and immunohistochemical staining were used to determine the Aβ deposition in both intracellular and extracellular neurons. Subsequently, the MCI-hub genes were verified by quantitative real-time PCR (qRT-PCR) in the peripheral blood of 3×Tg-AD mice. The research revealed ten hub genes associated with MCI were identified WGCNA. Short-term memory loss, intracellular Aβ deposition and limited of extracellular amyloid plaques in 3×Tg-AD mice. The qRT-PCR analysis of peripheral blood from these mice revealed significantly down-regulation in the expression levels of *ATP5C1, ITGB2, EFTUD2* and *RPS27A* genes; whereas the expression level of *VCP* gene was significantly up-regulated. These findings confirmed that 24-week-old male 3×Tg-AD mice were a valuable animal model for simulating the early symptomatic stages of AD. Additionally, the peripheral blood MCI-hub genes related to immune response, energy metabolism and ribosomal coding efficiency provide potential biomarkers for this stage.

Key words: Alzheimer's Disease, 3×Tg-AD mice, the early symptomatic stage, peripheral blood hub genes, weighted co-expression network analysis.

INTRODUCTION

Alzheimer's disease (AD) is a neurodegenerative disorder associated with the aging process. The diagnosis and intervention of the early stage of AD have emerged as the focus of clinical and medical research, given that timely intervention during this stage holds immense potential in slowing down the progression towards dementia (Editorial 2023). Symptomatic AD can be divided into mild cognitive impairment (MCI) and dementia stage, and MCI stage being considered as the early symptomatic phase of mouse AD models. Evidence increasingly highlights the early symptomatic stage of AD is the best period to identify and conduct treatment (Han et al. 2021, Alsen et al. 2022).

In recent years, the interaction between the central nervous system and peripheral organs has progressively emerged as a research hotspot in AD (Wu et al. 2023, Nelson 2022). The changes in the peripheral circulatory system occurred at MCI stage. Peripheral blood-based AD biomarkers might be more appropriate for mass screening and regular monitoring of disease's progression (Bhalala et al. 2024).

Bioinformatics is currently an effective tool for exploring key markers or pathogenesis

of diseases. Weighted gene co-expression network analysis (WGCNA) effectively identifies highly cooperative gene sets based on their interconnectivity and the correlation between these sets and phenotypes or therapeutic targets, thereby facilitating the identification of potential biomarker genes or therapeutic targets (Rangaraju et al. 2018).

The APP/PS1/tau triple-transgenic (3×Tg-AD) mice serve as an animal model for investigating the intricate pathogenic network of AD (Yan et al. 2023). Previous studies have defined 6-month-old 3×Tg-AD mice as being in early symptomatic stage of AD onset, and typical symptoms were observed in 9-month-old (Zhang et al. 2023). In the current study, we validated 24-week-old 3×Tg-AD mice to mimic the early symptomatic stage of AD. Meanwhile, the 10 hub genes were screened by WGCNA in peripheral blood of MCI patients from database (GSE63060, GSE63061) and identified by qRT-PCR in peripheral blood of 24-week-old male 3×Tg-AD mice respectively, which could potentially serve as biomarker for MCI.

MATERIALS AND METHODS

Screening of peripheral blood hub genes by Weighted gene co-expression network analysis

The WGCNA was performed per previous published method (Dai et al. 2021). In the current research, gene co-expression networks in the peripheral blood of MCI patients (datasets: GSE63060 and GSE63061), were analyzed by R software package. A summary of patient demographics can be found in Table I. First, the original data was preprocessed using the DESeq2 package in R language. Differentially expressed genes (DEGs) were identified based on a fold change (FC) cutoff criterion of > 1.5 and a false discovery rate (FDR) threshold of < 0.05. Next, the WGCNA package in R software was used to constructed and analyze a co-expression network of DEGs, where genes with high expression correlation were grouped into same modules based on their likely involvement in the biological processes or pathways. The intersection genes were identified from the modules most closely associated with the MCI stage from GSE63060 and GSE63061 datasets. Subsequently, Protein-Protein Interaction Networks (PPI) was constructed to investigate interaction genes and identify hub genes using the STRING online tool with an interaction score threshold set at 0.7. Visualization and analysis of this constructed network were performed using Cytoscape software v3.7.1. The hub genes were identified based on key parameters (degree, Maximum Neighborhood Component, Maximal Clique Centrality, etc.) by CytoHubba plugin within Cytoscape software.

Table I. Patient demographics of MCI in GSE63060 and GSE63061.

	Age	Females	Males	CDR-SOB
GSE63060				
Control (n = 67)	69.6 (±4.2)	41	26	0.07 (±0.18)
MCI (n = 39)	70.0 (±3.3)	24	15	1.24 (±1.60)
GSE63061				
Control (n= 71)	70.8 (±2.9)	44	27	0.15(±0.57)
MCI (n = 31)	69.5 (±4.5)	23	8	1.34 (±1.86)

Animals

The 3×Tg-AD mice (034830-JAX) and their breed-matched wildtype (WT) control mice (004807-JAX) were purchased from Jackson Laboratory (Bar Harbor, Maine). The mice were grouped (male: female = 1: 3) and housed in SPF grade animal room (Certificate No.: SYXK 2021-0003) for propagating newborn 3×Tg-AD and WT mice, allowed them free movement and eating. The genotypes of offspring mice were identified using PCR experiments, the primer sequences are shown in Table II. The 24-week-old mice were then used for subsequent experiments, as depicted in Figure 1. The ethical considerations for the animal experiment followed the Animal Care and Use Guidelines recommended by the EU (Directive 2101/63/EU) and were approved by the Animal Use and Care Committee of Zunyi Medical University [zyfy-an-2023-0301].

Y-maze

The mice were placed in the central area of Y-maze, and they were allowed free entry and exit from each arm within 10 min. The order and number of correct choices (i.e., entering A, B, C or A, C, B in sequence) was automatically analyzed by the TopScan behavioral analysis system. The free alternation rate (alternation %) was also statistically analyzed; the alternation correct rate (%) = counts of correct selections/ (total counts of arm piercings - 2) × 100%.

New object recognition

Prior to the experiment, the mice were allowed to habituate the environment for 10 min. The experiment is divided into familiarization period and testing period. During the familiarization period, the mice were freely explored the identical object for 5 min. After an interval of one hour, a novel object B with different color and shape replaced the initial object, and mice were allowed to freely explore for 5 min as well. Exploratory behavior was defined as the nose or front paws of mice contacting the object or pointing the object. The discrimination index

Table II. Primer sequences used for quantitative real-time PCR.

Gene	Sequence (5'-3')	Sequence (3'-5')
APP	AGGACTGACCACTCGACCAG	CGGGGGTCTAGTTCTGCAT
PS1	CACCCCATTCACAGAAGACA	CAACCCATAGGCAGGTCAAG
Tau	TGAACCAGGATGGCTGAG	TTGTCATCGCTTCCAGTCC
GAPDH	GTGGCAAAGTGGAGATTGTTG	CGTTGAATTTGCCGTGAGTG
ACTG1	CCCTAGCACCTAGCACGATG	GCCACCGATCCAGACTGAGT
EFTUD2	CTCCCCTCTCTATACCATCAAAGC	GAGTGCGGAGATCAGTCTCAAAG
RPS27A	CTATAAGGTGGATGAAAATGGC	TCTTCTGGTTTGTTGAAGCAGT
SOD1	CCAGTGCAGGACCTCATTTTAAT	TCTCCAACATGCCTCTCTTCATC
ATP5C1	AGTGGCTAAACAGATGAAGAATGAAG	TTCACCAACTCCAACAATCATAACTT
ITGB2	CAGGAATGCACCAAGTACAAAGT	CCTGGTCCAGTGAAGTTCAGC
RBX1	CCGAAGAGTGTACGGTTGCAT	CGTTTTGAGCCATCGAGAGAT
NFKBIA	CTCAAGAAGGAGCGCTTGGT	GCTCGTACTCCTCGTCCTTCAT
NFKB1	GCAACCAAAACAGAGGGGATTTC	TTTGACCTGTGGGTAGGATTTCTTG
VCP	TCTCAAACAGAAGAACCGACC	TCTTTCCTTTTAGCAACACCGT

(DI) was based on the time spent exploring the object B/ total exploration time.

Morris water maze

The test area was divided into four equal quadrants. A transparent platform was situated in the center of the third quadrant and 1 cm below the water surface. The mice were placed in the first, second, and fourth quadrants once a day for 4 consecutive days to test their spatial memory ability, and the escape latency was recorded within 60 s. If mice failed to reach the platform, they were guided onto the platform and stayed there for 15 s. The number of platform crossings was evaluated within 60 s during exploration experiment on day 5.

Tissue harvest

After conducting behavioral tests, 6 animals were randomly selected for perfusion fixation to perform Nissl staining and immunohistochemistry techniques, and peripheral blood RNA extracting for qPCR analysis. The mice were anesthetized with sodium pentobarbital (2%) intraperitoneally after behavioral tests. Once under complete anesthesia, blood samples were collected from their retro-orbital vein before being subjected to perfusion using a pre-cooled saline solution (200 mL) mixed with 4% paraformaldehyde. Subsequently, the brain tissue was then removed and fixed in 4% paraformaldehyde for 48 hours, before being dehydrated and paraffin-embedded.

Hematoxylin and eosin (HE) staining

The paraffin-embedded sections of mice brain were routinely dewaxed, and then stained with hematoxylin-eosin after dehydration with gradient ethanol.

Nissl Staining

The sections were routinely dewaxed and dehydrated, followed by a 10-min Nissl staining process. The surviving neurons had large cellular bodies and pale nuclei, while the dead neurons exhibited dark staining with shrunken cellular bodies. The surviving and damaged neurons were observed in three random fields (×400) of hippocampus CA1 and CA3 regions using upright optical microscope (Nikon Eclipse E100).

Immunohistochemical of intracellular Aβ

The sections were routinely dewaxed, block endogenous peroxidase activity, and block nonspecific binding. The sections were then incubated with anti-Aβ primary antibody (1:200, sc-28365, Santa Cruz Biotechnology, CA, USA) overnight at 4°C, which against Amyloid A4 including $Aβ_{1-42}$, $Aβ_{1-40}$ and other various lengths β-amyloid. After incubation, the sections were incubated with secondary antibody (1:200, E-IR-R217, Elabscienc, Wuhan, China) for 30 min. Immunoreactivity was observed after DAB color development and hematoxylin re-staining. In

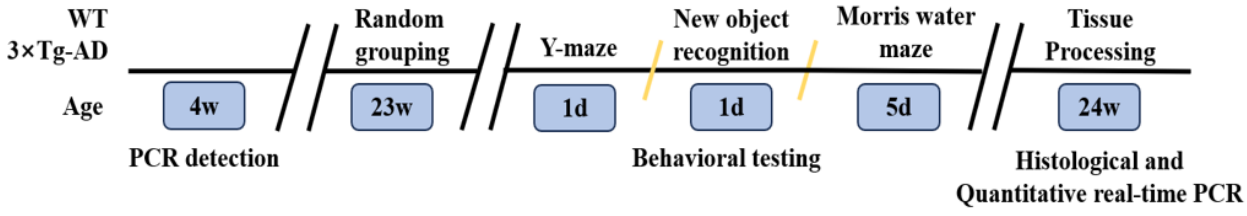

Figure 1. Experimental designs. WT: C57BL/6. W: Week. d: Day. Experimental program: mice were genotyped for tail detection at 4-week-old; The 23-week-old WT and 3×Tg-AD mice were grouped randomly, n=9 each group; Behavioral testing began at the start of week 23. Tissue harvest at 24-week-old.

three random fields (×400) of hippocampus CA1 and CA3 regions, the number of Aβ neurons were counted using Ortho-Fluorescent Microscopy (Nikon Eclipse C1).

Thioflavin-S staining

The sections were routinely dewaxed and dehydrated, followed by a 10-min incubation with 1% Thio-S in a dark environment. The Aβ plaque exhibited Thio-S^+ high-light granular structures within the remains of dead neurons. In three random fields (×400) of hippocampus, the number of Aβ plaques were counted using Ortho-Fluorescent Microscopy (Nikon Eclipse C1).

Identification of MCI-hub genes expression level in 3×Tg-AD mice blood by real-time PCR

Total RNA from WT and 3×Tg-AD mice peripheral blood was isolated using Whole Blood Purification Kit (K0761, Thermo Fisher Scientific Inc., USA). RNA concentration was measured by Nano Drop 2000 (Thermo Fisher Scientific, USA). And RNA was reverse transcribed using PrimeScript™ RT reagent Kit (RR037A, Takara Bio, China). The system of PCR reaction including SYBR Green 5 μL, cDNA 0.8 μL, primer mix (10 μM) 0.4 μL, and DEPC water 3.4 μL. PCR primers were purchased from Sangon Biotech (Shanghai, China) (Table I). The process was performed on CFX 96 real-time System (Bio-Rad, USA) using iTaq Universal SYBR Green Supermix (Thermo Fisher Scientific Inc., Shanghai, China). The cycling conditions were as follows: initial denaturation (95°C, 5 min), denaturation (40 cycles, 95 °C, 10 s), annealing (52°C, 30 s), and extension (72 °C, 20 s). The primer sequences are shown in Table II, and relative mRNA levels were normalized with GAPDH of each sample and calculated using the $2^{-\Delta\Delta}$CT formula.

Statistical analysis

The experimental data were analyzed using SPSS 29.0 statistical software. Data were presented as mean ± SD. The data normality distribution was tested using S-W test. If the data conform to a normal distribution, the water maze data were subjected to repeated measures analysis of variance, while the remaining data underwent a t-test for comparison between the two groups. Mann-whitney test was used for non-normal distribution data. $P < 0.05$ was considered a statistically significant difference.

RESULTS

Hub genes of MCI peripheral blood screened by WGCNA method

The Cluster Dendrogram plot and the Module-trait relationships plot show that the blue module in GSE63060 is highly positively correlated with MCI stage and is therefore selected as the module with the highest correlation. Meanwhile, the turquoise module in GSE63061 is also highly correlated with MCI stage (Figure 2a, b). PPI network analysis and was used to investigate the 292 intersecting genes between blue module in GSE63060 and turquoise module in GSE6306 (Figure 2c). The top 10 genes with the highest scores were identified and defined as hub genes by Cytoscape v3.7 software (Figure 2d).

Short-term memory deficits in 24-week-old 3×Tg-AD mice

The trends of prolonged escape latencies in the MWM test during training and reduced platform crossing number during exploration experiment were observed in 3×Tg-AD mice, but it was not statistically significant ($P = 0.661$, $F = 0.200$, $df = 1$) (Figure 3a, b, c). There were no significant differences of spontaneous alternation rate

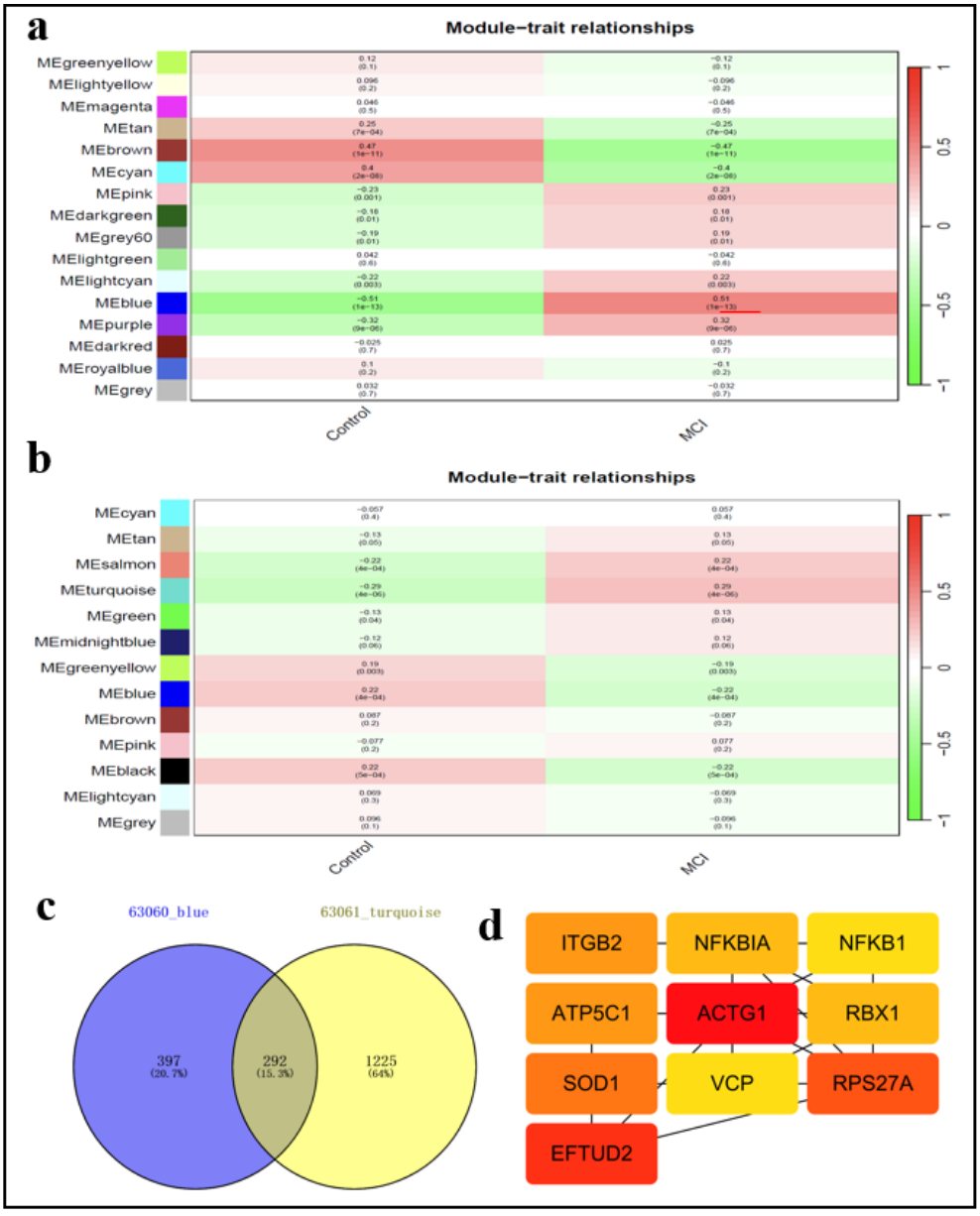

Figure 2. MCI-Hub genes in peripheral blood samples screened by WGCNA method. (a, b) Heap of module–trait relationships in AD dataset GSE63060 and GSE63061. (c) The intersecting genes between blue module in GSE63060 and turquoise module in GSE6306. (d) The MCI-hub genes identified by Cytoscape v3.7 software.

during Y-maze test (P>0.05) (Figure 3d). However, a reduced discrimination index was observed during the NOR test in 3×Tg-AD mice (P < 0.05) (Figure 3e). The results of NOR were considered to reflect short-term memory loss in 3×Tg-AD mice.

HE staining

The 24-week-old male 3×Tg-AD mice exhibited mild pathological damage in the hippocampus, as evidenced in Figure 4a, WT mice had a clear and complete cell structure and was densely arranged. However, small numbers of neurons with nuclear condensation were observed in the hippocampus of 3×Tg-AD mice.

Nissl staining

Nissl bodies, a characteristic structure in neuron, reflects the degree of neuronal atrophy or loss occurred in AD brain. There was a decreasing trend

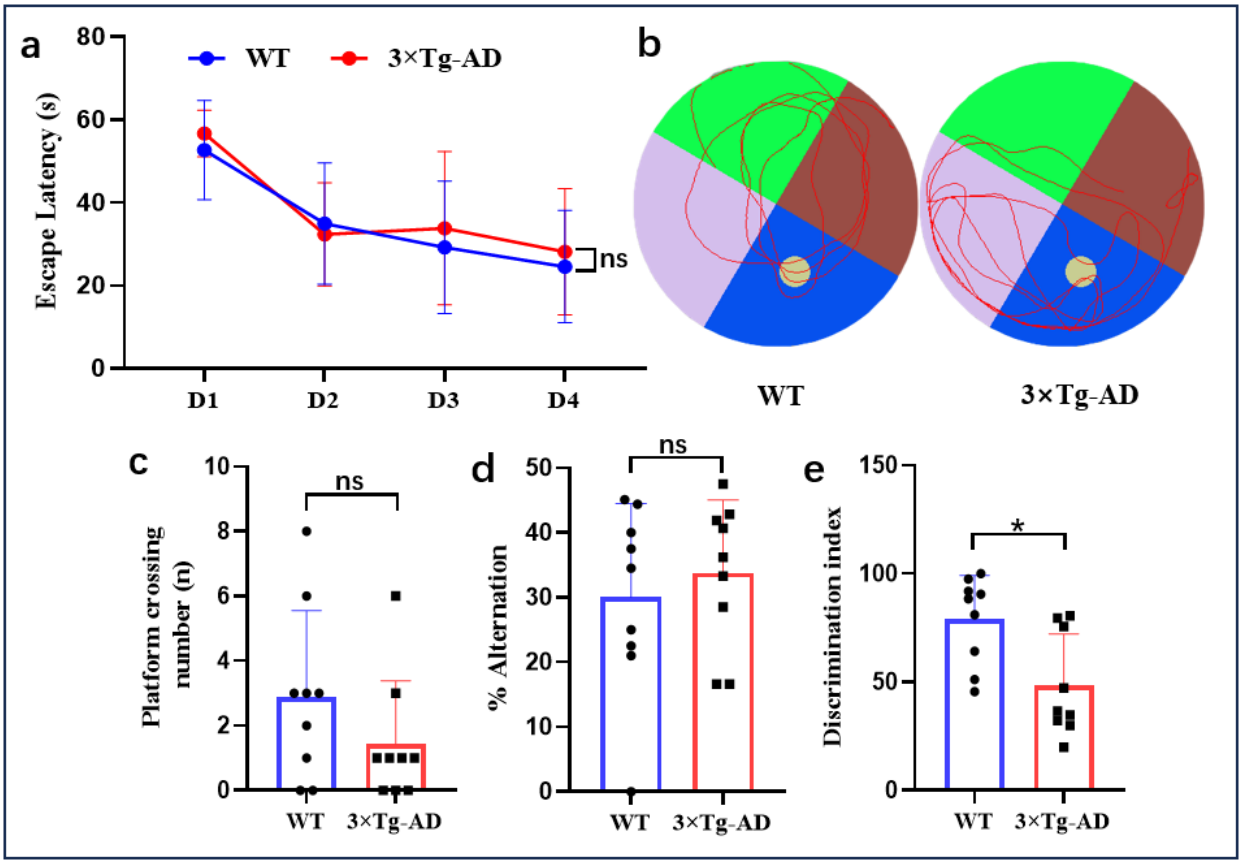

Figure 3. The behavioral tests (Y-maze, NOR, and MWM test) were performed at 23 weeks old; (a) Escape latency (seconds) in MWM test; (b) Representative images of trajectory diagram in spatial exploration. (c) The number of platform crossings in spatial exploration of MWM. (d) The alternation rate (%) in the Y-maze test. (e) The discrimination index in NOR test. Data were presented as mean ± SD with n = 9. *P < 0.05 compared with WT group. ns, not statistically significant.

in the total number of hippocampal neurons observed in 3×TG-AD mice. And an increased in dark neurons was observed in hippocampus CA1 and CA3 region of the hippocampus in 24-week-old 3×Tg-AD mice (Figure 4 b-d).

Aβ positive neuron increased in hippocampus of 24-week-old 3×Tg-AD mice

The Aβ positive neuron significantly increased in 24-week-old 3×Tg-AD mice (P<0.05) (Figure 5a, c). These findings suggest that intracellular Aβ increasing may occur before the formation of extracellular Aβ plaque and it represents an early pathogenic event in AD.

Extracellular amyloid plaque disposition in hippocampus

The data showed a small number of brain neurons are positive for Thioflavin-S staining. However, no extracellular amyloid plaques deposition in 3×Tg-AD mice. The results indicate that extracellular Aβ plaques did not accumulate in significant during the early symptomatic stage of AD (Figure 5b).

Real-time PCR method for validation of hub genes

The hub genes identified by WGCNA were validated in the peripheral blood of 24-week-old male 3×Tg-AD mice, the results are shown

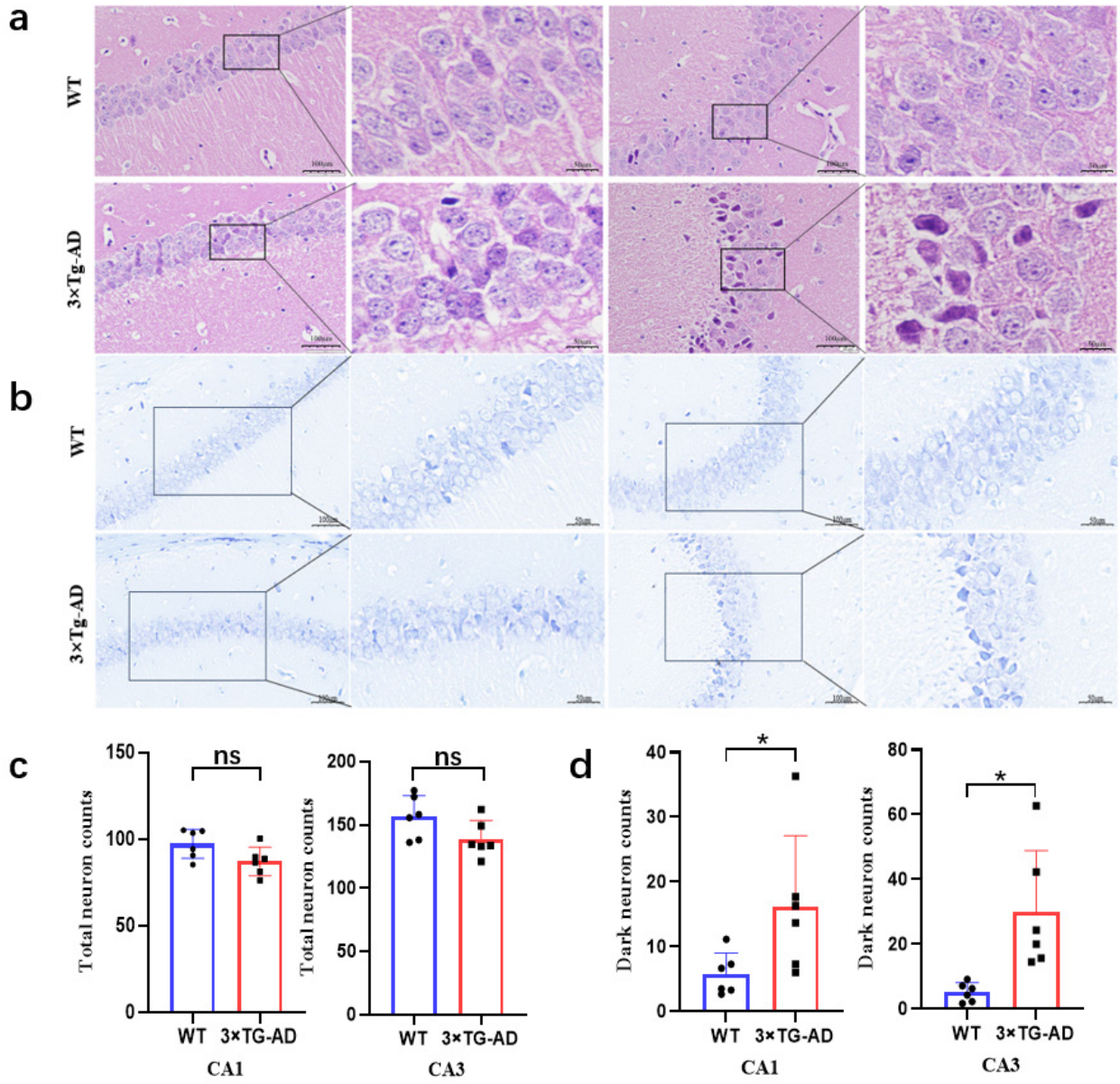

Figure 4. Hippocampal morphology in 24-week-old WT and 3×Tg-AD mice. (a) Representative images of HE staining; (b) Representative images of Nissl staining; (c) Total surviving neuron in hippocampus (Nissl staining). (d) Total dark neurons in hippocampus (Nissl staining). Data are presented as mean ± SD with n = 6. *P < 0.05 compared with WT group.

in Figure 6. Compared with the WT group, the expression levels of *ATP5C1*, *ITGB2*, *EFTUD2* and *RPS27A* were downregulated, while *VCP* was upregulated in 24-weeks-old 3×Tg-AD mice. However, no significant differences were observed in the expression levels of *NFKB1*, *RBX1*, *SOD1*, *ACTG1* and *NFKBIA* genes.

DISCUSSION

AD is a very complex disorder mediated by dysfunctional central-peripheral communication and coordination, never an internal problem of brain (Bettcher et al. 2021). The objective of this research is to identify peripheral blood biomarkers in MCI stage. WGCNA is an analytical

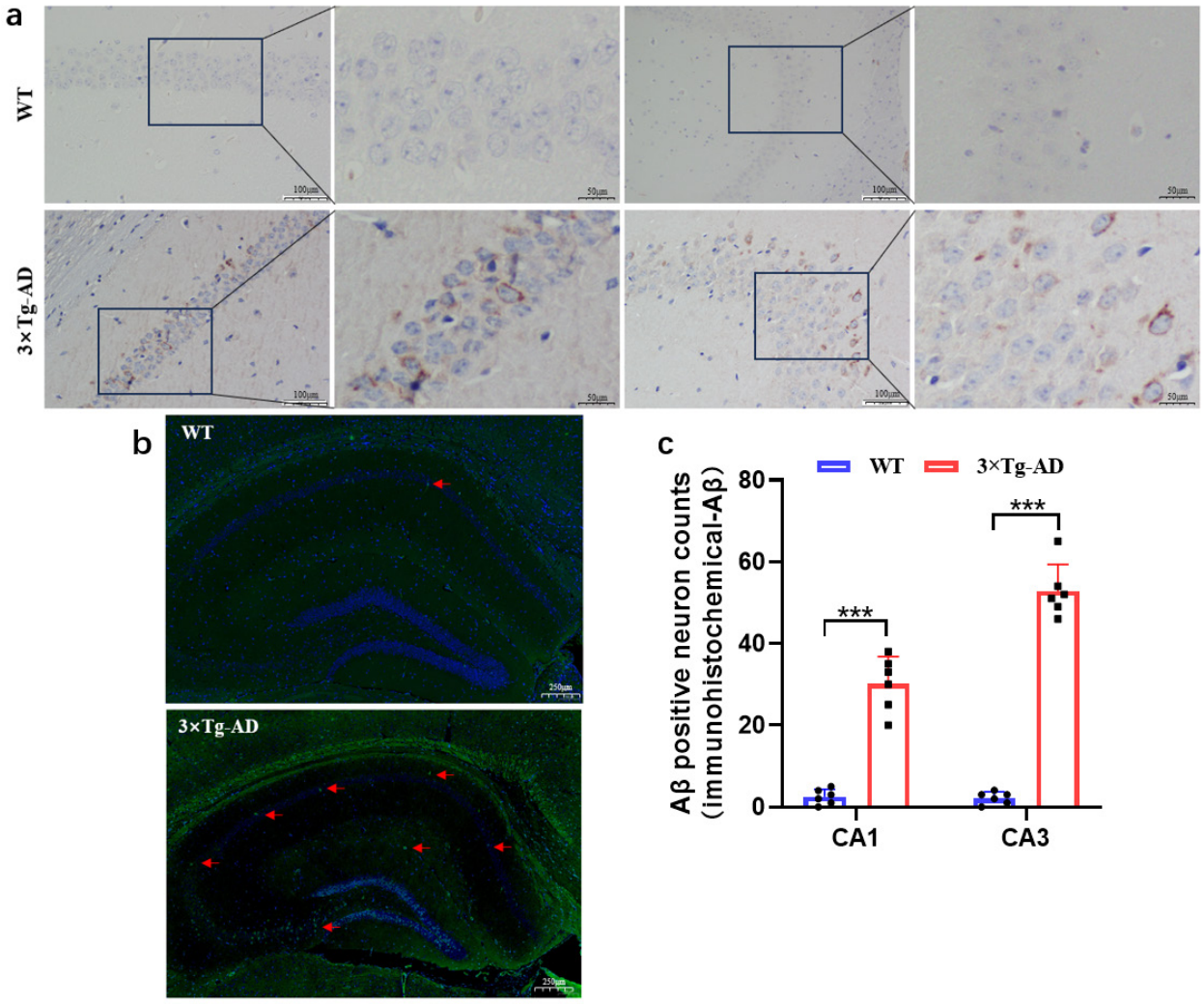

Figure 5. The extracellular and intracellular Aβ deposition in Hippocampus. (a) Representative images of immunohistochemical-Aβ (n = 6). (b) Representative images of Thio-S staining, small red arrows represent Aβ positive neuron (green) and DAPI (blue). (c) The number of Aβ positive neuron in hippocampus (immunohistochemical-Aβ). Data are presented as mean ± SD with n = 6. $^{***}P$<0.001 compared with WT group. The red arrows represent Aβ-positive neurons in the thioflavin stain.

method that effectively establishes correlations among genes, samples, gene modules, and biological traits. It is particularly suited for analyzing large and complex sample sets to facilitate the identification and screening of crucial modules and key genes associated with specific clinical phenotypes. In this study, ten MCI-hub genes (*ATP5C1*, *ITGB2*, *EFTUD2*, *RPS27A*, *VCP*, *NFKB1*, *RBX1*, *SOD1*, *ACTG1* and *NFKBIA*) were identified using WGCNA method for subsequent qRT-PCR verification.

The results are consistent with previous research and indicate that limited short-term memory loss only by NOR in 24-week-old 3×Tg-AD mice. However, the MWM and Y-maze primarily reflect deficits in reference memory, which typically manifest during the stage of moderate cognitive impairment in mouse models of AD (Webster et al. 2014). These findings could be explained that cognitive deficit have not yet manifested in 24-week-old male 3×Tg-AD mice,

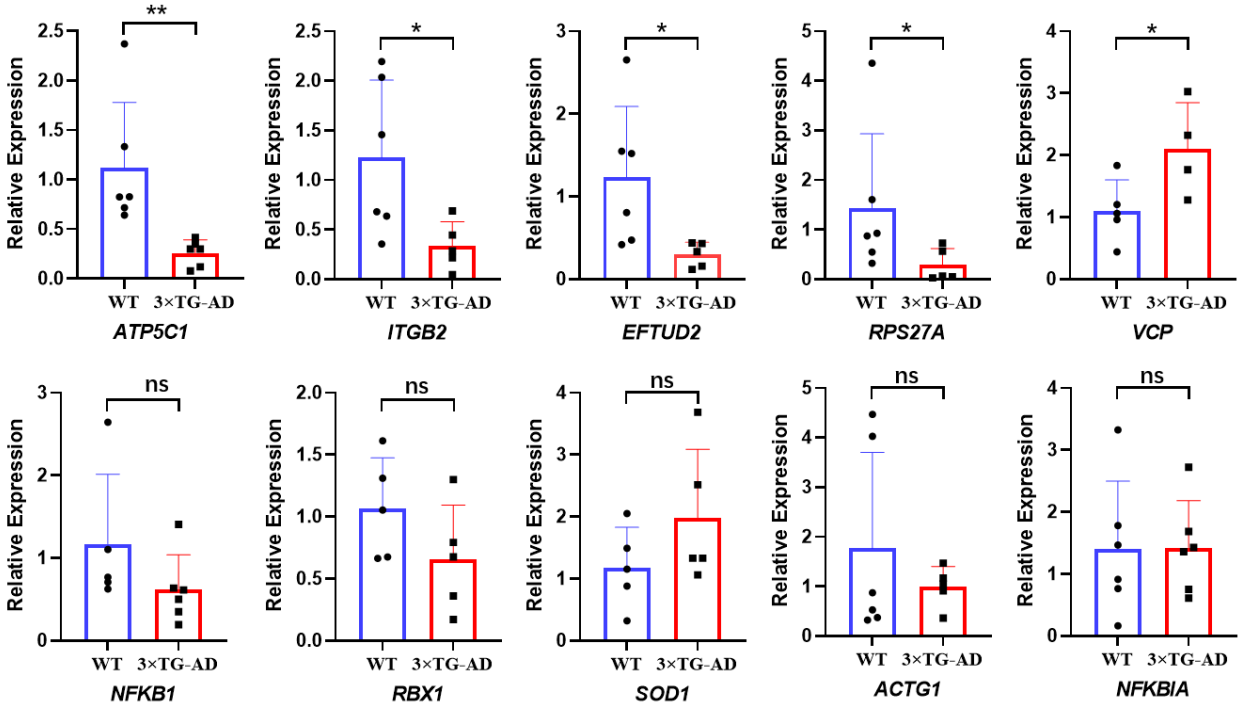

Figure 6. The expression levels of *ATP5C1*, *ITGB2*, *EFTUD2*, *RPS27A*, *VCP*, *NFKB1*, *RBX1*, *SOD1*, *ACTG1*, *NFKBIA* genes in peripheral blood of WT mice and 3×Tg-AD mice. Data are presented as mean ± SD with n = 4-6; $^{*}P < 0.05$ compared with WT group, $^{**}P < 0.01$ compared with WT group.

which were considered in early symptomatic stage of AD pathology.

The presence of intracellular Aβ in neurons is observed at an earlier stage, preceding the formation of visible Aβ plaques (Oddo et al. 2003). The "core" of concentrated amyloid is formed inside a single intact neuron, which then degenerates to form extracellular Aβ plaques (Lee et al. 2022). The findings of this study revealed mild neuronal damage and increased Aβ-positive neurons was observed in the hippocampus of 24-week-old 3×Tg-AD male mice, without the presence of characteristic extracellular Aβ plaques, indicate that Aβ remains primarily deposited in neuronal cells, at least in the 24-week-old 3×Tg-AD mice (Zhang et al. 2020). Moreover, in comparison to thioflavin-S staining, Immunohistochemistry staining exhibited enhanced sensitivity towards Aβ and enabled earlier detection of Aβ in neurons. Indicating increased neuron intracellular Aβ levels are important biomarkers for identifying the early symptomatic stages of AD.

The increased of neuronal necrosis during the pre-symptomatic phase, and a subsequent decrease during dementia stage (Tanaka et al. 2020). Furthermore, the formation of Aβ plaques serve as a neuroprotective mechanism by facilitating the aggregation of soluble Aβ into Aβ fibrinopeptides, thereby mitigating its toxicity (Huang et al. 2021). This finding is consistent with the observed pattern of neuronal injury in current study and suggests that targeting soluble brain Aβ during the MCI stage holds promise for therapeutic interventions against AD.

Our group has found that AD patients exhibited peripheral immune cell dysfunction, and that the increase in Aβ burden in the early stages of AD mice under B cell depletion

conditions was significantly increased (Xiong et al. 2021). The presence of peripheral immune cells in the brains of healthy humans and animal model indicate that the brain is not an isolated immune organ (Rustenhoven et al. 2021). The abnormal increase of soluble Aβ in peripheral circulation leads to immune dysfunction, resulting in impaired immune surveillance and reduced Aβ clearance capacity (Schwartz & Baruch 2014). In this study, the expression levels of *ITGB2*, *EFTUD2* were found to be down-regulated in peripheral blood of 24-weeks-old 3×Tg-AD mice, while *VCP* was up-regulated. *ITGB2*, which encodes the integrin β chain, is implicated in immune cell adhesion and plays a role in regulating macrophage infiltration into the brain (Lin et al. 2022). Additionally, it represents a potential co-pathogenic factor for both diabetes and AD (Shu et al. 2020). EFTUD2, encoding the elongation factor Tu GTP binding domain-containing protein 2, has been identified as a crucial modulator of innate immunity (Zhu et al. 2015). Over expression of EFTUD2 has been shown to enhance immune surveillance and peripheral immune cell response (Yang et al. 2023), but its pathogenic mechanism in AD remains unreported. *VCP*, encoding Valosin-containing protein, has been identified as a pathogenic gene associated with frontotemporal dementia, and involvement in aging and AD (Wang et al. 2019). Specifically, VCP can inhibit the complement system and impair defense mechanisms (Jha & Kotwal 2003). The results suggest that peripheral immunity may be abnormal in the early stages of AD.

Impairment of energy metabolism represents a prominent and profound alteration in AD, which is closely associated with accelerated aging (González et al. 2022). Interestingly, the age-related cognitive decline can be reversed by reprogramming myeloid cell metabolism (Minhas et al. 2021). This study reveals that the expression level of *ATP5C1* gene is down-regulated in the peripheral blood of 24-weeks-old male 3×Tg-AD mice, indicating abnormal peripheral energy metabolism. Additionally, *RPS27A* encoding and regulating ribosomal proteins, the expression levels were significantly downregulated in 24-week-old 3×Tg-AD mice, could indicate the decreased efficacy of encoding ribosomal proteins in the peripheral blood of AD patients.

The analyses revealed that the hub genes primarily participate in immune response, energy metabolism, and efficacy of encoding ribosomal proteins, suggesting their potential pivotal role in the pathogenesis of the MCI stage. These findings highlight their promising prospects as novel targets for the prevention and treatment of AD. However, there are also several deficiencies as follows: Firstly, due to the limited availability of blood samples from WT and 3×Tg-AD mice, we obtained only enough for qRT-PCR detection but not sufficient for Western blot analysis of MCI-hub gene proteins in peripheral blood. Furthermore, the current study used 24 weeks of age in 3×Tg-AD mice to simulate the early stage of AD and identified MCI-hub genes; However, it did not ascertain the dementia-Hub gene in elderly 3×Tg-AD mice, thereby limiting exploration of differential expression patterns of hub genes in peripheral blood across different stages of AD. Therefore, it is important to acknowledge that there are certain limitations in our findings. However, future studies will address these mentioned limitations.

Acknowledgments

The authors thanks P. Liu Jie and P. Li Fei for intellectual guidance. D. He Fang for weighted gene co-expression network analysis.

REFERENCES

AISEN P, JIMENEZ-MAGGIORA G, RAFII M, WALTER & RAMAN R. 2022. Early-stage Alzheimer disease: getting trial-ready. Nat Rev Neurol 18(7): 389-399.

BETTCHER B, TANSEY M, DOROTHE G & HENEKA M. 2021. Peripheral and central immune system crosstalk in Alzheimer disease - a research prospectus. Nat Rev Neurol 17(11): 689-701.

BHALALA O, WATSON R & YASSI N. 2024. Multi-Omic Blood Biomarkers as Dynamic Risk Predictors in Late-Onset Alzheimer's Disease. Int J Mol Sci 25(2): 1231.

DAI L, XIE Y, ZHANG W, ZHONG X, WANG M, JIANG H, HE Z, LIU X, ZENG H & WANG H. 2021. Weighted Gene Co-Expression Network Analysis Identifies ANGPTL4 as a Key Regulator in Diabetic Cardiomyopathy via FAK/SIRT3/ROS Pathway in Cardiomyocyte. Front Endocrinol (Lausanne): 12705154.

EDITORIAL: 2023. 2023 Alzheimer's disease facts and Figures. Alzheimers Dement 19(4): 1598-1695.

GONZALEZ A, CALFIO C, CHURRUCA M & MACCIONI RB. 2022. Glucose metabolism and AD: evidence for a potential diabetes type 3. Alzheimers Res Ther 14: 56.

HAN S, ZHANG M, JEON YY, MARGOLIS DJ & CAI Q. 2021. The role of mitophagy in the regulation of mitochondrial energetic status in neurons. Autophagy 7(12): 4182-4201.

HUANG YT, HAPPONEN KE, BURROLA PG, O'CONNOR C, HAH N, HUANG L, NIMMERJAHN A & LEMKE G. 2021. Microglia use TAM receptors to detect and engulf amyloid β plaques. Nat Immunol 22(5): 586-594.

JHA P & KOTWAL GJ. 2003. Vaccinia complement control protein: multi-functional protein and a potential wonder drug. J Biosc 28: 265-271.

LEE J ET AL. 2022. Faulty autolysosome acidification in Alzheimer's disease mouse models induces autophagic build-up of Aβ in neurons, yielding senile plaques. Nat Neurosci 25(6): 688-701.

LIN C, XU C, ZHOU Y, CHEN A & JIN B. 2022. Identification of Biomarkers Related to M2 Macrophage Infiltration in Alzheimer's Disease. Cells 11: 2365.

MINHAS PS ET AL. 2021. Restoring metabolism of myeloid cells reverses cognitive decline in ageing. Nature 590: 122-128.

NELSON A. 2022. Peripheral Pathways to Neurovascular Unit Dysfunction, Cognitive Impairment, and Alzheimer's Disease. Front Aging Neurosci 18(14): 858429.

ODDO S, CACCAMO A, SHEPHERD JD, MURPHY MP, GOLDE TE, KAYED R, METHERATE R, MATTSON MP, AKBARI Y & LAFERLA FFM. 2003. Triple-transgenic model of Alzheimer's disease with plaques and tangles: intracellular Abeta and synaptic dysfunction. Neuron 39(3): 409-421.

RANGARAJU S ET AL. 2018. Identification and therapeutic modulation of a pro-inflammatory subset of disease-associated-microglia in Alzheimer's disease. Mol Neurodegener 13(1): 24.

RUSTENHOVEN J ET AL. 2021. Functional characterization of the dural sinuses as a neuroimmune interface. Cell 184: 1000-1016.

SCHWARTZ M & BARUCH K. 2014. Breaking peripheral immune tolerance to CNS antigens in neurodegenerative diseases: boosting autoimmunity to fight-off chronic neuroinflammation. J Autoimmun 54: 8-14.

SHU J, LI N, WEI W & ZHANG L. 2020. Detection of molecular signatures and pathways shared by Alzheimer's disease and type 2 diabetes. Gene 810: 146070.

TANAKA H ET AL. 2020. YAP-dependent necrosis occurs in early stages of Alzheimer's disease and regulates mouse model pathology. Nat Commun 11(1): 507.

WANG G ET AL. 2019. Mutation and association analyses of dementia-causal genes in Han Chinese patients with early-onset and familial Alzheimer's disease. J Psychiatr Res 113: 141-147.

WEBSTER SJ, BACHSTETTER AD, NELSON PT, SCHMITT FA & VAN ElLDIK LJ. 2014. Using mice to model Alzheimer's dementia: an overview of the clinical disease and the preclinical behavioral changes in 10 mouse models. Front Genet 5: 88.

WU Y ET AL. 2023. Hepatic soluble epoxide hydrolase activity regulates cerebral Aβ metabolism and the pathogenesis of Alzheimer's disease in mice. Neuron 111(18): 2847-2862.

XIONG LL ET AL. 2021. Single-cell RNA sequencing reveals B cell-related molecular biomarkers for Alzheimer's disease. Exp Mol Med 53(12): 1888-1901.

YAN F ET AL. 2023. Icariin ameliorates memory deficits through regulating brain insulin signaling and glucose transporters in 3×Tg-AD mice. Neural Regen Res 18(1): 183-188.

YANG GC, SHI Y, FAN CN, LI Y, YUAN MQ, PEI J, WU Y & WU HT. 2023. Spliceosomal GTPase Eftud2 regulates microglial activation and polarization. Neural Regen Res 18: 856-862.

ZHANG J, HUA XF, GU JH, CHEN F, GU JL, GONG CX, LIU F & DAI CL. 2020. High Mobility Group Box 1 Ameliorates Cognitive

Impairment in the 3×Tg-AD Mouse Model. J Alzheimers Dis 74(3): 851-864.

ZHANG W, LI D & SHI J. 2023. Alterations of Spatial Memory and Gut Microbiota Composition in Alzheimer's Disease Triple-Transgenic Mice at 3, 6, and 9 Months of Age. Am J Alzheimers Dis Other Demen 38: 15333175231174193.

ZHU C, XIAO F & LIN W. 2015. EFTUD2 on innate immunity. Oncotarget 6: 32313-32314.

How to cite
LIU H, YU C & QIN C. 2024. The changes of peripheral blood hub genes in 24-week-old APP/PS1/Tau triple transgenic mouse model based on weighted gene co-expression network analysis. An Acad Bras Cienc 96: e20240120. DOI 10.1590/0001-3765202420240120.

Manuscript received on February 06, 2024
accepted for publication on May 06, 2024

HEXU LIU[1]
https://orcid.org/0009-0004-3734-9537

CHANGYIN YU[2]
https://orcid.org/0000-0002-4529-9750

CHAO QIN[1]
https://orcid.org/0000-0002-9965-2142

[1]First Affiliated Hospital of Guangxi Medical University, Department of Neurology, No. 6 ShuangYong Road, Nanning 530021, Guangxi Autonomous Region, China

[2]Affiliated Hospital of Zunyi Medical University, Department of Neurology, No. 149 Dalian Road, Zunyi 563000, Guizhou Province, China

Correspondence to: **Chao Qin**
E-mail: chaoqin202012@163.com

Author contributions

Qin C, Yu C-Y contributed to design of study, data collection, analysis, and interpretation of results; Liu H-X given substantial contributions to the data collection and analysis. Yu C-Y, manuscript editing. All authors have participated to drafting the manuscript, author Qin Chao revised it critically. All authors read and approved the final version of the manuscript and agree with the order of presentation of the authors.